Journal of Materials Science & Technology 178 (2024) 39–47

Contents lists available at ScienceDirect

Journal of Materials Science & Technology

journal homepage: www.elsevier.com/locate/jmst

Research Article

Creep rupture life prediction of high-temperature titanium alloy using cross-material transfer learning

Changlu Zhou[a], Ruihao Yuan[a,b,*], Baolong Su[a], Jiangkun Fan[a], Bin Tang[a], Pingxiang Zhang[a], Jinshan Li[a,b,*]

[a] State Key Laboratory of Solidification Processing, Northwestern Polytechnical University, Xi'an 710072, China
[b] Chongqing Innovation Center, Northwestern Polytechnical University, Chongqing 401120, China

ARTICLE INFO

Article history:
Received 26 June 2023
Revised 12 August 2023
Accepted 27 August 2023
Available online 8 October 2023

Keywords:
Machine learning
Transfer learning
Creep rupture life
High-temperature titanium alloy

ABSTRACT

High-temperature titanium alloys are the key materials for the components in aerospace and their service life depends largely on creep deformation-induced failure. However, the prediction of creep rupture life remains a challenge due to the lack of available data with well-characterized target property. Here, we proposed two cross-materials transfer learning (TL) strategies to improve the prediction of creep rupture life of high-temperature titanium alloys. Both strategies effectively utilized the knowledge or information encoded in the large dataset (753 samples) of Fe-base, Ni-base, and Co-base superalloys to enhance the surrogate model for small dataset (88 samples) of high-temperature titanium alloys. The first strategy transferred the parameters of the convolutional neural network while the second strategy fused the two datasets. The performances of the TL models were demonstrated on different test datasets with varying sizes outside the training dataset. Our TL models improved the predictions greatly compared to the models obtained by straightly applying five commonly employed algorithms on high-temperature titanium alloys. This work may stimulate the use of TL-based models to accurately predict the service properties of structural materials where the available data is small and sparse.

1. Introduction

High-temperature titanium alloys are beneficial for reducing the weight of components in aerospace [1–4], due to their lightweight and good mechanical properties at elevated temperatures. Their operation temperatures can range from 400 to 650 °C [5–7] and the lifetime for different components can change from hundreds to even tens of thousands of hours [3]. The service life of the high-temperature components largely depends on the creep behavior, as indicated by the permanent plastic deformation under applied stress before yielding [8]. As a result, many attentions are being paid to the assessment of the creep behavior, in particular, the creep rupture life. Generally, the creep property can be evaluated by measuring the evolution of strain as a function of time under certain stress and temperature. However, such measurements are often time-intensive and costly due to the long-period essence and the harsh thermal-mechanical coupling service environment. This then motivates the development of prediction methods/models for the creep property, by examining its dependence on compositions, processing, microstructures, and testing conditions.

Several empirical and theoretical methods have been presented to predict the creep rupture life, such as time-temperature parameter methods and continuum damage models [9–14]. Using the time-temperature parameter method, Bolton [9,10] forecasted the creep rupture life of CrMo, CrMoVNb, 304H, and Incoloy 800 alloys via extrapolation. The continuum models for predicting creep behavior developed rapidly in recent years with the advance of crystal plasticity theory and continuum mechanics [11–14]. They were usually combined with descriptors that relate to creep deformation and microstructures to simulate and predict the stress rupture properties. For example, an improved damage mechanics approach was developed to simulate the stress rupture properties of single-crystal superalloys [11]. Beyond the time-temperature parameter method that bases itself only on the measured stress and temperature, creep continuum models that consider microstructures can provide physical insights [15–20] into the understanding of creep behaviors. However, both methods still lead to non-negligible deviations between the predictions and measurements. Furthermore, they are often not readily applied to new alloys as the composition and processing have not been taken into account for modeling.

* Corresponding authors at: State Key Laboratory of Solidification Processing, Northwestern Polytechnical University, Xi'an 710072, China.
E-mail addresses: rhyuan@nwpu.edu.cn (R. Yuan), ljsh@nwpu.edu.cn (J. Li).

https://doi.org/10.1016/j.jmst.2023.08.046
1005-0302/

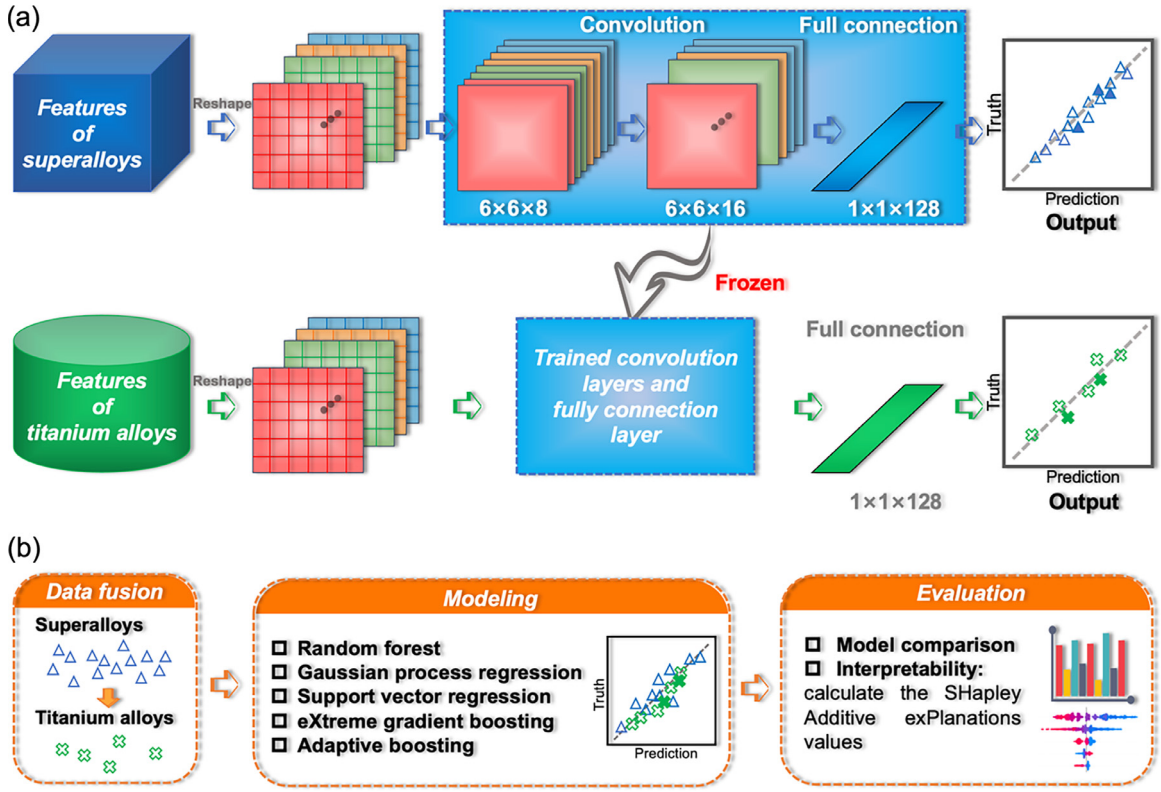

Fig. 1. Schematic diagram of transfer learning for predicting creep rupture life of high-temperature titanium alloy using Fe-base, Ni-base, and Co-base alloys knowledge transfer. (a) Parameter transfer, (b) data fusion-based transfer.

Machine learning (ML) can automatically discover patterns and laws underlying materials data to construct composition-processing-structure-property mapping, which can then generalize to unknown data to make predictions and has been widely used to assist materials discovery [21–24]. It has also been used to predict the creep properties of metallic structural materials where datasets of a relatively large size can be utilized [25–30]. By introducing thermodynamics-calculated microstructural information as inputs, ML-based surrogate models were established for predicting the creep rupture life of Fe-base high-temperature alloys [26]. The creep rupture life of Ni-base single-crystal superalloys was predicted by fusing clustering algorithms, thermodynamic calculations, and regression models [31]. The surrogate models in these studies often require a large dataset to ensure their robustness. However, compared to the well-studied superalloys and steels, the available dataset for high-temperature titanium alloys is generally of quite limited size. Therefore, this does not allow us to train a robust surrogate model for predicting the creep rupture life via directly applying ML algorithms on such small dataset.

We in this study presented two transfer learning (TL) strategies to predict the creep rupture life of high-temperature titanium alloys that are effective for very sparse experimental dataset. TL uses relevant techniques to transfer the knowledge learned from one task with a large dataset to improve the surrogate model for another task with a small dataset. It has been employed in various fields to mitigate the issues caused by small datasets [32–34]. For example, it was shown that for semiconductors, by using TL the prediction of phonon properties can be largely improved by leveraging a larger dataset of electron properties [35]. In these studies, the properties can be either different or the same, but the large and small datasets are often constituted by the same materials. For some selected materials such as high-temperature titanium alloys, a large dataset is unavailable and impedes the application of TL. Here we shall show that using the knowledge obtained from a large dataset of Ni-base, Co-base, and Fe-base superalloys, one can greatly improve the prediction of creep rupture life for high-temperature titanium alloys. Our strategy includes two cross-materials TL methods, the first uses convolutional neural network (CNN) framework by which the pre-trained parameters based on Fe-base, Ni-base, and Co-base alloys were employed to train the model for high-temperature titanium alloys, as shown in Fig. 1(a). The second fuses the superalloys dataset with high-temperature titanium alloys to improve the predictive model for creep rupture life (Fig. 1(b)).

2. Methods

2.1. Dataset and data preprocessing

The source dataset of the large size used in this paper was obtained from the public NIMS database https://cds.nims.go.jp/. The dataset includes 753 samples across Fe-base, Ni-base, and Co-base alloys with experimentally measured creep rupture life (data.S1.csv in Supporting Information). To detect outliers in the dataset, we conducted PCA and K-means clustering on the dataset of Fe-base, Ni-base, and Co-base superalloys, as shown in Fig. S1 in the Supplementary Material. All 753 samples were well clustered and no outliers were found. Each sample is described by 33 features such as chemical compositions (22 elements), heat treatment processing (9 parameters), experimental conditions (2), *etc.* (Table S1). The distribution of the creep rupture life of these alloys was analyzed (Fig. S2). The target dataset of limited size was collected manually from Refs. [5,36–45]. There are in total 88 samples characterized by 25 features (Table 1 and data.S2.csv in Supporting Information). Compared to the source data, the target dataset is

Table 1
Features and property of the high-temperature titanium alloys. Min and Max represent the largest and smallest value of each feature.

	Inputs and output	Min	Max	Mean	Standard deviation
Inputs	Ti (mass%)	82.95	89.74	85.95	2.13
	C (mass%)	0	0.1	0.06	0.03
	Si (mass%)	0	0.46	0.24	0.17
	Ni (mass%)	0	0.7	0.15	0.29
	Mo (mass%)	0	0.8	0.36	0.25
	W (mass%)	0	1	0.07	0.24
	Al (mass%)	5.75	6.61	5.97	0.24
	N (mass%)	0	0.05	0.01	0.01
	Nb+Ta (mass%)	0	1.4	0.55	0.41
	B (mass%)	0	0.11	0.01	0.02
	V (mass%)	0	4.23	1.25	1.88
	Fe (mass%)	0	1.18	0.16	0.34
	Zr (mass%)	0	4	2.44	1.63
	Sn (mass%)	0	4.02	2.74	1.83
	Solution Treatment Time (h) (ST_Tim)	0	2	0.80	0.92
	Solution Treatment Temperature (°C) (ST_Tem)	0	1080	685.48	481.28
	Solution Treatment Cooling Way (ST_CW)	0	3	0.74	0.63
	Aging Treatment Time (h) (AT_Tim)	0	50	2.77	8.39
	Aging Treatment Temperature (°C) (AT_Tem)	0	770	467.01	328.54
	Aging Treatment Cooling Way (AT_CW)	0	1	0.67	0.47
	2nd Aging Treatment Time (h) (2_AT_Tim)	0	50	1.14	7.45
	2nd Aging Treatment Temperature (°C) (2_AT_Tem)	0	610	13.86	90.91
	2nd Aging Treatment Cooling Way (2_AT_CW)	0	1	0.02	0.15
	Test Temperature (°C) (TT)	475	675	603.41	47.40
	Test Stress (MPa) (TS)	97	550	283.86	89.75
Output	Creep Rupture Life (h)	0.00157	4770	299.01	792.33

*Cooling way: 1 (air cooling), 2 (oil cooling), 3 (water cooling), 4 (furnace cooling).

rather small. The distribution of the features and property are shown in Fig. S3. All the features do not distribute uniformly and most creep rupture life biases to small values. We used the logarithm of the property, *i.e.*, lg(creep rupture life), as the output in both datasets because it conforms more to the normal distribution and can improve the performance of ML models. In addition, all the features were normalized by the Max-Min method to avoid the influence of different magnitudes of features on the models.

2.2. Transfer learning

There are two TL strategies. In the first strategy (Fig. 1(a)), a source CNN model was trained on a large dataset and then applied to a small dataset. To facilitate the construction of CNN-based TL model, we used 34 features which are the union set of features from both large and small datasets, as input. The features unavailable were filled with zero. First, the 34-dimensional features were reshaped into a 6×6 matrix in turn, and the values of the last two elements of the matrix were filled with zero. Matrixes of different shapes, that is, 4×9 and 5×7 were compared, and the 6×6 matrix performs the best. The CNN parameters were set as follows, the first convolutional layer is $6 \times 6 \times 8$, the second convolutional layer is $6 \times 6 \times 16$, the full connection layer is $1 \times 1 \times 128$, and the filter size is 2×2. The loss function (mean squared error) was optimized using the Adam optimizer and the learning rate is 0.005. The model was obtained after 1500 epochs. In the second strategy (Fig. 1(b)), the two datasets were fused together to train the surrogate model for creep rupture life, and five commonly used algorithms were used. Similar to the first strategy, we used all 34 features to describe the creep rupture life. All the algorithms were implemented in Python using TensorFlow or Scikit-learn.

Three commonly employed statistical indicators were used to evaluate the model performance, that is, the coefficient of determination (R^2), mean absolute error (MAE), and mean square error (MSE). Their definitions are given by,

$$R^2 = 1 - \frac{\sum_{i=1}^{n} \left(y_i - \hat{y}_i\right)^2}{\sum_{i=1}^{n} \left(y_i - \bar{y}\right)^2}, \tag{1}$$

$$\mathrm{MAE} = \frac{1}{n} \sum_{i=1}^{n} \left|\hat{y}_i - y_i\right|, \tag{2}$$

$$\mathrm{MSE} = \frac{1}{n} \sum_{i=1}^{n} \left(y_i - \hat{y}_i\right)^2, \tag{3}$$

where y_i and $\hat{y}_i$ indicate the actual and predicted values, respectively. The $\bar{y}$ is the mean of y_i and n is the number of samples in the dataset.

3. Results

3.1. Models for titanium alloys by directly applying typical ML algorithms

Five commonly used ML algorithms include Random Forest (RF), Support Vector Regression (SVR), eXtreme Gradient Boosting (XGBoost), Gaussian Process Regression (GPR), and Adaptive Boosting (AdaBoost) were used to train the surrogate models for predicting the creep rupture life of high-temperature titanium alloys. The model performance was evaluated by three indexes on the test dataset, *i.e.*, R^2, MAE, and MSE. We herein not used the random division to split the training and test dataset as this method is not enough to measure the extrapolation of the surrogate models. Instead, we divided the initial 88 samples into training and test data by considering the test temperature (T) and test stress (S). Specifically, there are five divisions and the corresponding test datasets are given by, $T \leq 600$ °C and $S \geq 450$ MPa (7 samples), $T \leq 600$ °C and $S \geq 400$ MPa (11), $T \leq 600$ °C and $S \geq 350$ MPa (20), $T \leq 600$ °C and $S \geq 300$ MPa (38), and $T \leq 600$ °C and $S \geq 250$ MPa (49). The performances of the five models are listed

Table 2
Performance of the five typical ML algorithms-based surrogate models.

Samples in test data	Training/test samples ratio	Evaluation index	Typical ML algorithms				
			RF	SVR	XGBoost	GPR	AdaBoost
$T \leq 600$ °C, $S \geq 450$ MPa	81/7	R^2	0.8108	0.7769	0.7474	0.6114	0.5095
		MAE	0.4646	0.5776	0.4793	0.7678	0.7854
		MSE	0.3566	0.4206	0.4762	0.7325	0.9247
$T \leq 600$ °C, $S \geq 400$ MPa	77/11	R^2	0.7009	0.6815	0.5599	0.5054	0.4455
		MAE	0.5696	0.5982	0.6826	0.7347	0.7267
		MSE	0.3931	0.4186	0.5784	0.6501	0.7289
$T \leq 600$ °C, $S \geq 350$ MPa	68/20	R^2	0.7047	0.7229	0.7834	0.6415	0.4897
		MAE	0.4934	0.4979	0.3977	0.5153	0.5695
		MSE	0.3274	0.3073	0.2402	0.3976	0.5658
$T \leq 600$ °C, $S \geq 300$ MPa	50/38	R^2	0.1979	0.5797	0.1991	0.3765	0.2634
		MAE	0.8919	0.7485	0.8645	0.7086	0.8755
		MSE	1.4023	0.7347	1.4	1.0901	1.2877
$T \leq 600$ °C, $S \geq 250$ MPa	39/49	R^2	0.5193	0.4925	0.4127	0.4334	0.5833
		MAE	0.7489	0.6802	0.8034	0.7683	0.7214
		MSE	0.9884	1.0436	1.2076	1.1651	0.8568

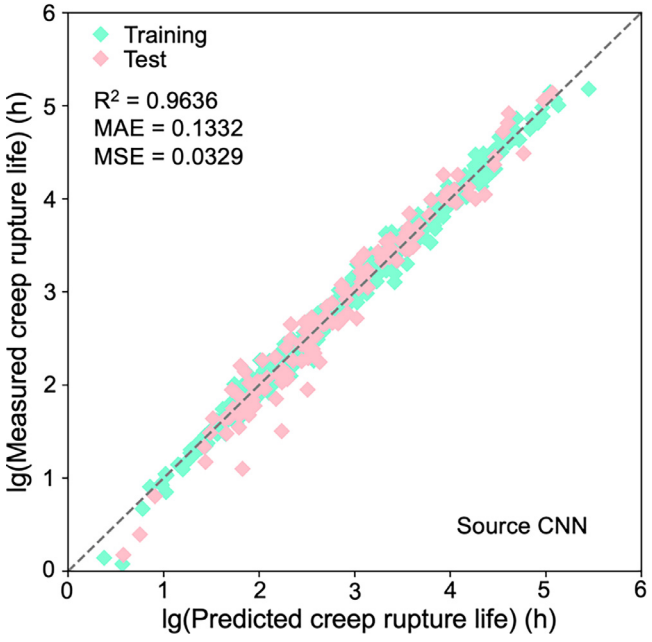

Fig. 2. Performance of the source CNN model based on the large source dataset of 753 samples.

in Table 2, all the values of the three indexes were calculated on the test dataset. It is seen that the highest R^2 (0.81) is for the 7 samples with $T \leq 600$ °C and $S \geq 450$ MPa, not adequate for a robust and accurate model. However, the highest R^2 for the 38 samples and 49 samples is only ~0.58, far from satisfactory. This is reasonable as it is accepted that the larger the data used to train the surrogate model, the better the model performance. We shall next show how to improve such models by utilizing the TL strategies.

3.2. Models for titanium alloys using CNN-based TL

Before building the target model (TrCNN) for titanium alloys, we first trained a source CNN model based on the large dataset of Ni-base, Co-base, and Fe-base samples. The performance of the source model is shown in Fig. 2. It can be seen that all the data points are distributed close to the diagonal line. We next calculated the three indexes to quantitatively evaluate the model performance. To avoid bias in data division, we randomly split the 753 samples 20 times with a ratio of 8:2 and trained 20 models. The average R^2 on the test dataset reaches ~0.96, indicating that it has the potential to build a robust TrCNN model for predicting the creep rupture life of titanium alloys.

We next transferred the CNN model parameters to titanium alloys by using the frozen convolution and full connection layers. A new full connection layer was added to obtain the predicted property, and the corresponding weights were randomly initialized and optimized via 1500 epochs. The performances of the TrCNN model for different training and test datasets are shown in Fig. 3. It is seen that the R^2 (test data) of the TrCNN models for $T \leq 600$ °C and $S \geq 450$ MPa (Fig. 3(a)), $T \leq 600$ °C and $S \geq 400$ MPa (Fig. 3(b)), and $T \leq 600$ °C and $S \geq 350$ MPa (Fig. 3(c)) are about 0.93, 0.91, and 0.84, much higher than that obtained by the five typical algorithms in Table 2. In Fig. 3(d, e), the samples in the training data are close to the diagonal line while those in the test data deviate from the diagonal line. This suggests that the models are overfitting. Nonetheless, compared to the best typical ML models, *i.e.*, SVR (R^2~0.58) and AdaBoost (R^2~0.58) in these two cases, the performance of TrCNN models has still been largely improved (R^2~0.79). Fig. 4 compares the TrCNN models to the five typical ML models. In all cases, the TrCNN owns the highest R^2, the lowest MSE, and MAE. Thus, with the help of the source model architecture, we are able to capture better the underlying tendency behind the high-temperature titanium alloys. It can be seen that with the stress used to separate out the test data decreases, the performance of the model (on test data) degenerates. This can be mainly ascribed to the amount of samples in the training and test data, with the stress increases, the number of samples in the test data decreases, and that in the training data increases. In general, the larger the training data size is, the more accurate the resulting model on the test data.

It is shown that our TL-based models perform rather well on the data of titanium alloys, which can be ascribed to the similarity in the mechanisms underlying the creep behaviors. It is well known that different alloys have differing mechanisms, however, the mechanisms have similarity in specific conditions. For example, in some conditions the slip of dislocations dominates and in others the diffusion of atoms may play the key role. To the best of our knowledge, there is no explicit criterion that when TL can be used on different kinds of datasets. It was argued that there might be no material properties as being completely independent, and every property might bear some dependencies on others directly or indirectly [33]. One possible way to quantitatively guide the use of TL may be from the data science view, such as the assessment of model similarity by comparing the model parameters

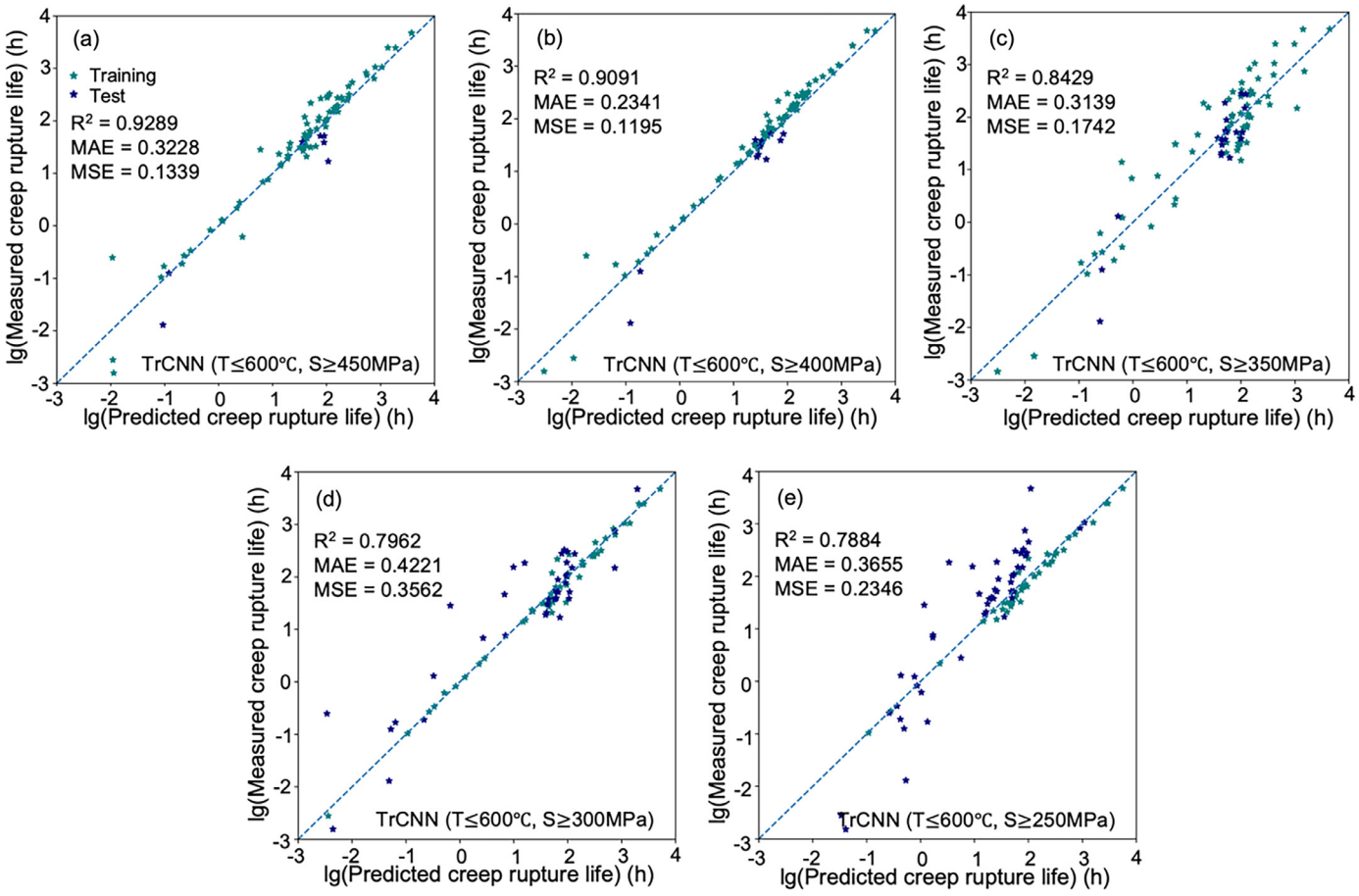

Fig. 3. Performance of the TrCNN models on different test datasets. (a) $T \leq 600$ °C, $S \geq 450$ MPa, (b) $T \leq 600$ °C, $S \geq 400$ MPa, (c) $T \leq 600$ °C, $S \geq 350$ MPa, (d) $T \leq 600$ °C, $S \geq 300$ MPa, and (e) $T \leq 600$ °C, $S \geq 250$ MPa.

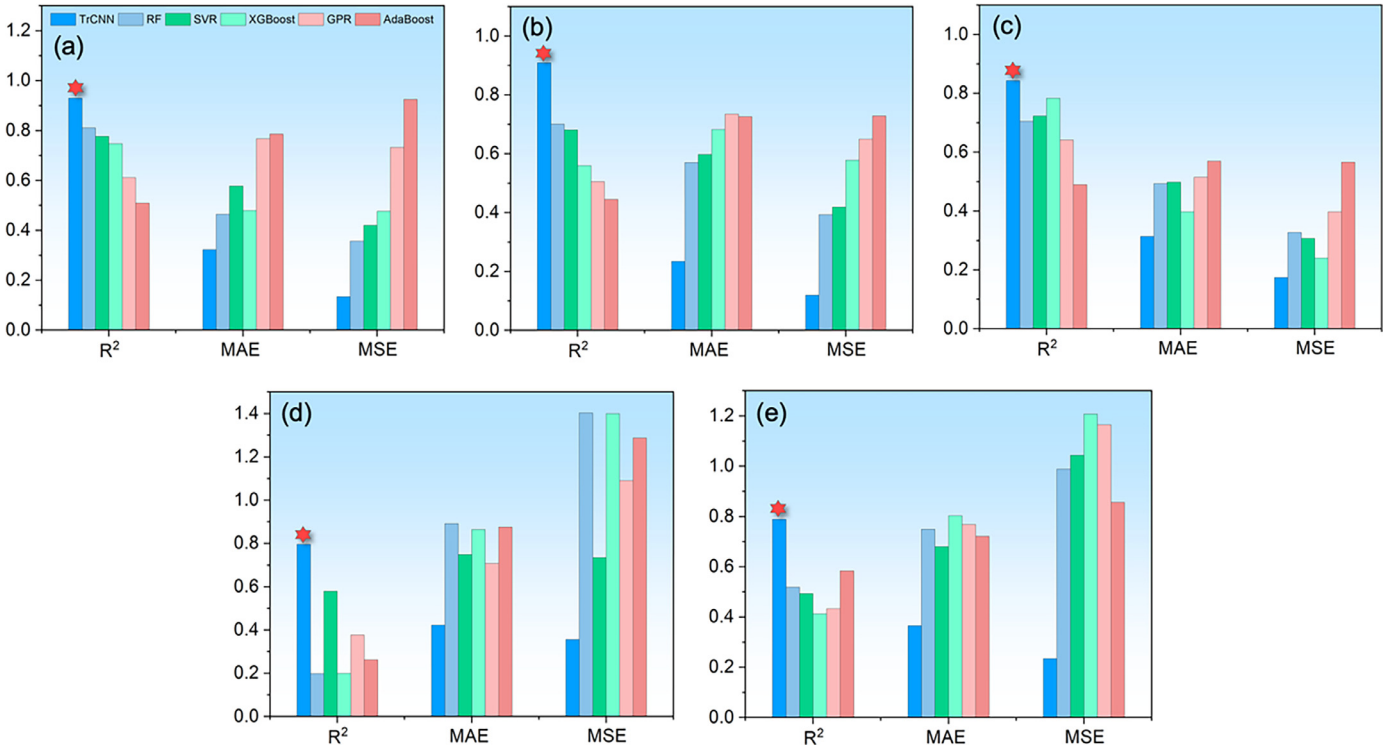

Fig. 4. Performance comparison between TrCNN and typical ML models on different test datasets. (a) $T \leq 600$ °C, $S \geq 450$ MPa, (b) $T \leq 600$ °C, $S \geq 400$ MPa, (c) $T \leq 600$ °C, $S \geq 350$ MPa, (d) $T \leq 600$ °C, $S \geq 300$ MPa, and (e) $T \leq 600$ °C, $S \geq 250$ MPa.

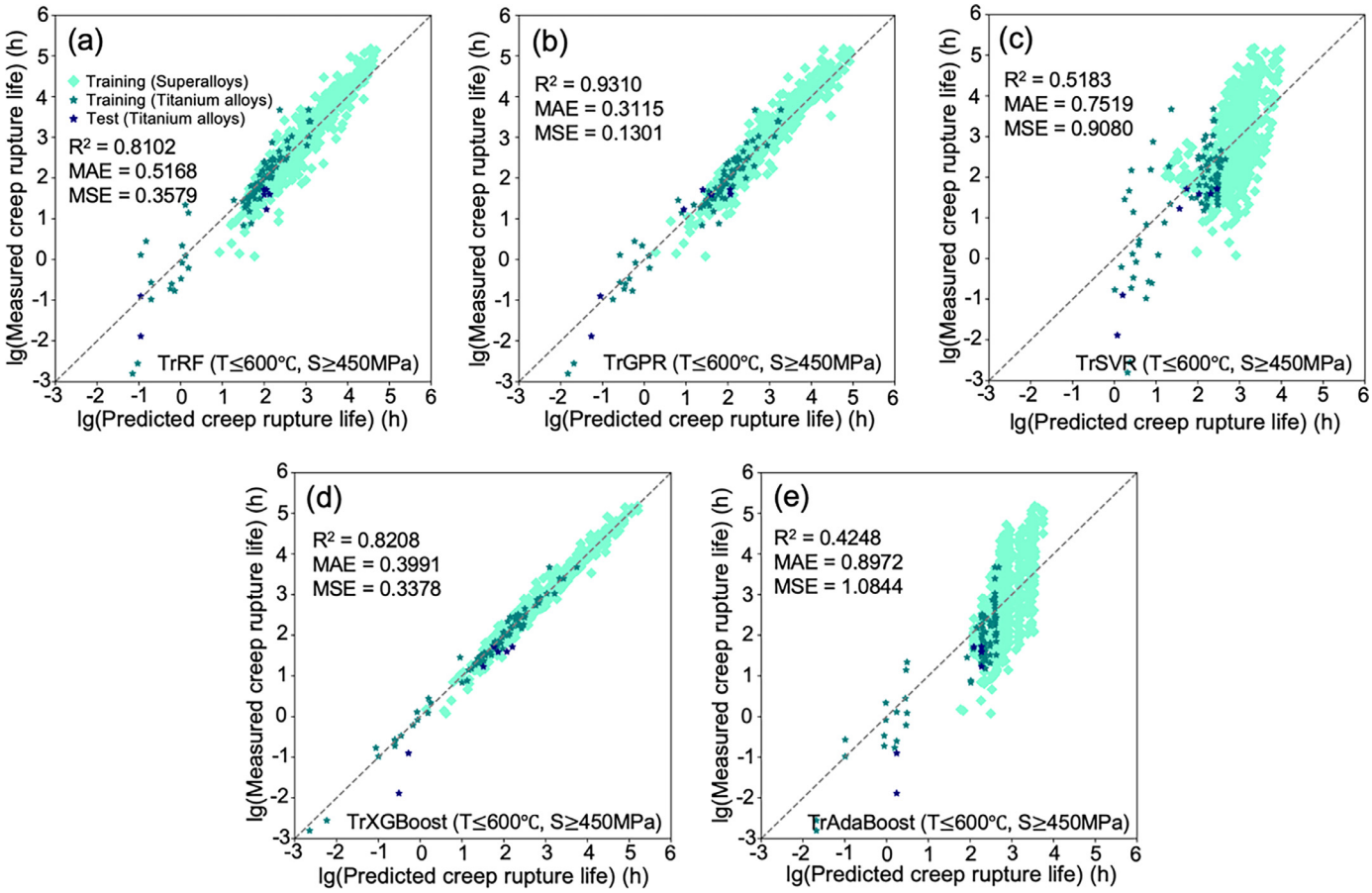

Fig. 5. Performance of the data fusion-based TL models on the test dataset of $T \leq 600$ °C and $S \geq 450$ MPa. (a) TrRF, (b) TrGPR, (c) TrSVR, (d) TrXGBoost, and (e) TrAdaBoost.

on different kinds of data. The higher similarity in model parameters might indicate that there exists a larger correlation between different datasets.

3.3. Models for titanium alloys using data fusion-based TL

We directly combined the two datasets of large and small size to train the ML models for the creep rupture life of titanium alloys. The same five algorithms (abbreviated as TrRF, TrGPR, TrSVR, TrXGBoost, and TrAdaBoost) were used and the corresponding model performance is shown in Figs. 5 and S4–S7. As an example, Fig. 5 shows the performance of different models on the test dataset of $T \leq 600$ °C and $S \geq 450$ MPa. Interestingly, not all the models were improved after data fusion. For example, the R^2 (~0.93) of TrGPR was largely improved compared to the original GPR model (R^2~0.61, Table 2) without data fusion. However, the R^2 of TrAdaBoost is only ~0.42, even lower than the AdaBoost (R^2~0.51, Table 2). This suggests that some algorithms can effectively make use of the knowledge learned from the large dataset but some cannot.

Fig. 6 compares the model performance before and after data fusion. The models obtained from data fusion-based TL on 4/5 test datasets perform better than the models without data fusion, except for the one under condition, $T \leq 600$ °C and $S \geq 250$ MPa. Fig. 6(a–d) shows that the optimal TL model differs on different test datasets. Specifically, the corresponding optimal models are TrGPR, TrGPR, TrXGBoost, and TrXGBoost, respectively. This further verified that there is no universal model that is suitable for all cases [46]. The bad performance of the TL model in Fig. 6(e) can be ascribed to the fact that the decreasing number of titanium alloys in the training data. In this case, the number of alloys in the test dataset (49) is more than that in the training dataset (39).

4. Discussion

4.1. Stability evaluation of TrCNN model

Based on the above analysis, both the TrCNN model and the data fusion-based TL models perform better than the ML models trained directly on the titanium alloys. In particular, the TrCNN model improves the accuracy to the largest degree. In order to verify the stability of the TrCNN model on small/sparse dataset, we examined the model performance as a function of the number of alloys. Specifically, the number of alloys in the new dataset varies from 20 % to 100 % (the initial 88 samples) by random sampling. To make the results statistically meaningful and reliable, we randomly divided the new dataset into training and test datasets with a ratio of 8:2 by 20 times and built the corresponding TrCNN models. Fig. 7 shows the model performance as a function of the number of samples in the new dataset. The typical ML models were also included as a comparison. The error bars were obtained by averaging the indexes of the 20 trained models for each new dataset. As the size of the new dataset increases, the model performance improves and becomes stable when the size is larger than 35. In terms of all three indexes, the TrCNN model always has the highest R^2, the lowest MAE, and MSE. Furthermore, the error bars of the TrCNN models are much lower than those of the typical ML models, especially when the new dataset size is small.

To determine how the TL-based model performs in predicting superalloys with different magnitudes of creep rupture life, we di-

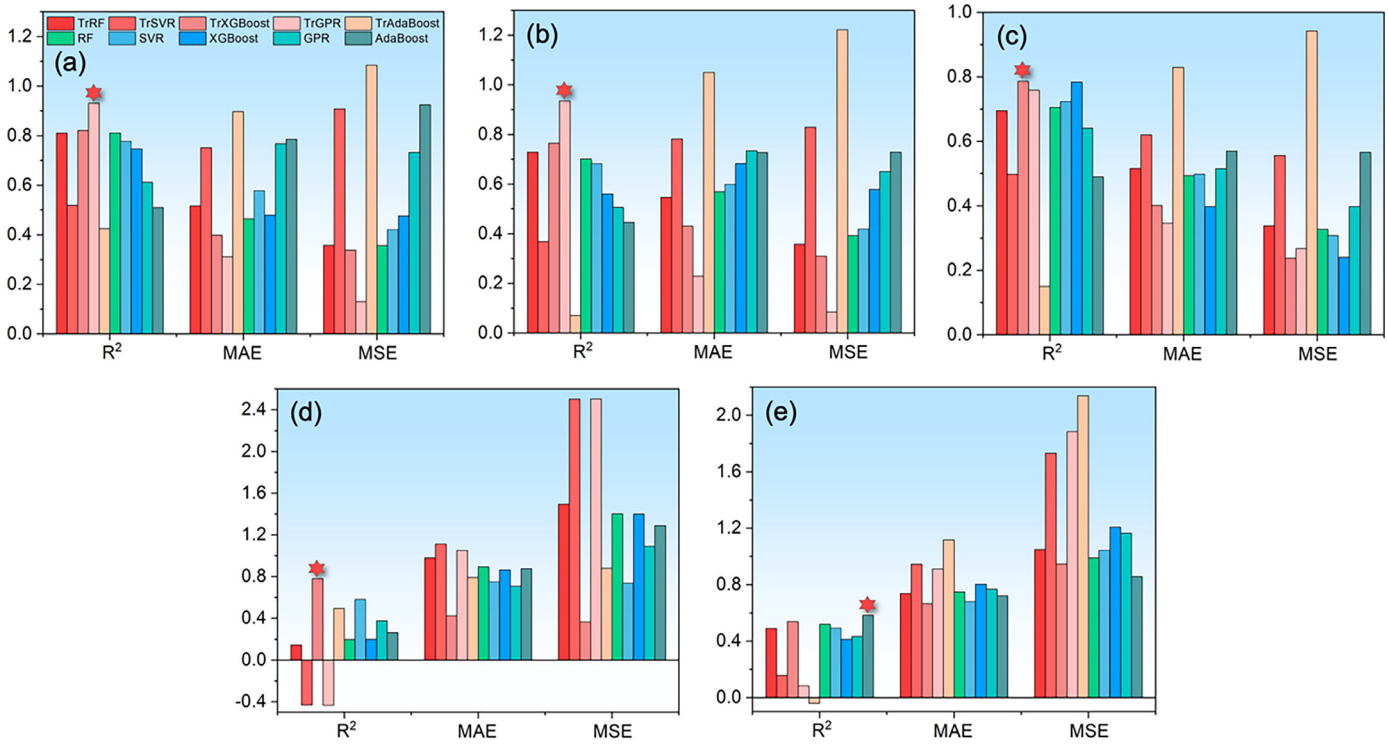

Fig. 6. Performance comparison between data fusion-based TL and typical ML models. (a) $T \leq 600$ °C, $S \geq 450$ MPa, (b) $T \leq 600$ °C, $S \geq 400$ MPa, (c) $T \leq 600$ °C, $S \geq 350$ MPa, (d) $T \leq 600$ °C, $S \geq 300$ MPa, and (e) $T \leq 600$ °C, $S \geq 250$ MPa.

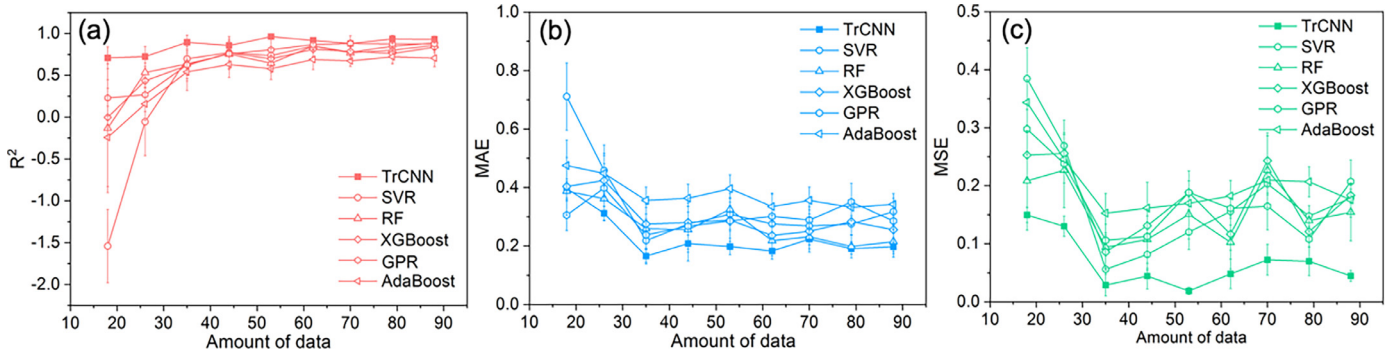

Fig. 7. Performance comparison of TrCNN and typical ML models by randomly dividing the training and test datasets with different ratios. (a) R^2, (b) MAE, (c) MSE on the test dataset.

vided the 88 samples into three groups with varying creep rupture life of 0–1 h, 1–200 h, and 200–5000 h. The TrCNN was trained using all 88 samples and then applied to the three groups, and Fig. S8(a–c) shows the performance of the corresponding models. It can be seen that the R^2 for the first two groups is higher than 0.9 and for the third group is about ~0.85, suggesting that the TrCNN model performs better on the superalloys with relatively short creep rupture life.

4.2. Interpretable analysis for the improved TL models

We next used SHAP (SHapley Additive exPlanation) analysis to gain insight into how data fusion can improve the accuracy of predictions. The TrGPR model on the test dataset ($T \leq 600$ °C, $S \geq 400$ MPa) was taken as an example as it shows the highest R^2. As a comparison, the corresponding GPR model was also included. Fig. 8(a, b) shows the impact of features on the predictions for the TrGPR and GPR models, respectively. The first ten features were listed for simplicity. For both models, the test temperature (TT) and test stress (TS) rank highly and this is reasonable considering that these two attributes serve as the key parameters in the empirical time-temperature methods to predict creep rupture life [47]. The features TT and TS *vs* their SHAP values in Fig. 8(a) distribute much more uniform than that in Fig. 8(b). This hints that, for each sample, the impact of the feature on the SHAP value (increase or decrease the prediction) is distinct. For the ML algorithm, this is important because different samples should encode varying information. In contrast, for the GPR model, many points cluster together, which means that different sample encodes the same information. Therefore, it is sound for us to deduce that the fusion of different datasets may help adjust the weight of each titanium alloy sample when training ML algorithms and finally improve the model performance. We also did a SHAP analysis of only titanium alloys on the predictions for the TrGPR model, as shown in Fig. S9. The distribution of SHAP values in Fig. S9 is similar to that in Fig. 8(a), further indicating that fusing different datasets indeed helps adjust the weight of each titanium alloy sample and improves the model performance. In addition, we also analyzed the coupling effect of each two feature on the predictions, as shown in Fig. 8(c, d). In both models, the effect between TT and TS is much

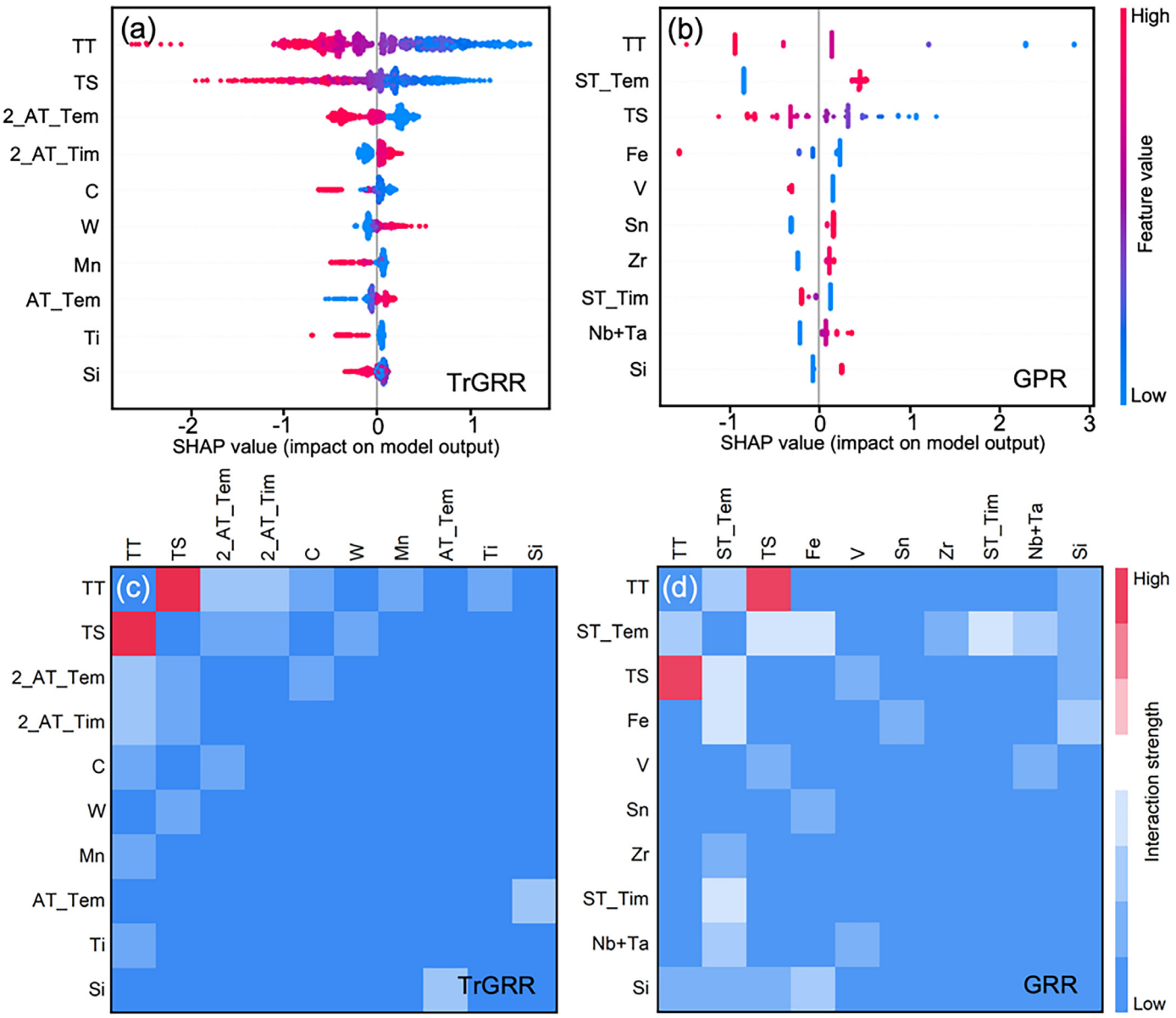

Fig. 8. SHAP analysis showing the feature impact on the prediction for the TrGPR model (a, c), and the corresponding GPR model (b, d).

higher than the others. Fig. 8(c) shows that TT combined with 2nd aging treatment temperature (2_AT_Tem) and time has a relatively large coupling effect. By contrast, Fig. 8(d) suggests that solution treatment temperature (ST_Tem) with TS has a high effect on the predictions.

Previous studies showed that the compositions, processings, and test conditions largely affect the creep behavior and rupture life. The SHAP analysis shows that except for TT and TS, the heat treatment parameters such as the ST_Tem and aging treatment temperature (AT_Tem) also rank highly. This is because these parameters affect the microstructures and influence the creep behavior. For example, with increasing ST_Tem the volume fraction of incoherent α-β interfaces decreases and the creep resistance is enhanced [48]. Similarly, Si can improve the creep resistance by solid solution strengthening and formation of silicides [49,50].

5. Conclusion

In summary, we presented two cross-material TL strategies to improve the prediction of creep rupture life of high-temperature titanium alloys. The first strategy trained a CNN-based model using the Fe-base, Ni-base, and Co-base superalloys and transferred the parameters to high-temperature titanium alloys. The established TL model improved the predictions greatly compared to the typical ML models obtained by directly applying the relevant algorithms on high-temperature titanium alloys. The second strategy fused the superalloys and titanium alloy datasets together to train the ML models. It was found that the performance of models based on the fused dataset also surpasses the ones straightly on the small dataset of high-temperature titanium alloys. The robustness of the TL models was confirmed by examining their extrapolation capability on test datasets of different sizes and distributions. The results suggested that the TL models are quite suitable for the sparse dataset and can shed light on other studies where the predictions are inadequate due to the lack of enough data.

Data and code availability

The data and codes are uploaded to the author's github repository: https://github.com/materials-informatics-nwpu/Cross-materials-transfer-learning.

Declaration of Competing Interest

The authors declare that they have no known competing financial interests or personal relationships that could have appeared to influence the work reported in this paper.

Acknowledgments

This work was financially supported by the National Key Research and Development Program of China (No. 2021YFB3702604) and the National Natural Science Foundation of China (No. 52002326).

Supplementary materials

Supplementary material associated with this article can be found, in the online version, at doi:10.1016/j.jmst.2023.08.046.

References

[1] H. Liu, H. Wang, L. Ren, D. Qiu, K. Yang, J. Mater. Sci. Technol. 132 (2023) 100–109.
[2] P.F. Gao, M.W. Fu, M. Zhan, Z.N. Lei, Y.X. Li, J. Mater. Sci. Technol. 39 (2020) 56–73.
[3] R.R. Boyer, Mater. Sci. Eng. A 213 (1996) 103–114.
[4] P. Singh, H. Pungotra, N.S. Kalsi, Mater. Today-Proc. 4 (2017) 8971–8982.
[5] M.J.R. Barboza, C.M. Neto, C.R.M. Silva, Mater. Sci. Eng. A 369 (2004) 201–209.
[6] P. Pototzky, H.J. Maier, H.J. Christ, Metall. Mater. Trans. A 29 (1998) 2995–3004.
[7] Z.X. Zhang, J.K. Fan, B. Tang, H.C. Kou, J. Wang, X. Wang, S.Y. Wang, Q.J. Wang, Z.Y. Chen, J.S. Li, J. Mater. Sci. Technol. 49 (2020) 56–69.
[8] C.X. Cui, B.M. Hu, L.C. Zhao, S.J. Liu, Mater. Des. 32 (2011) 1684–1691.
[9] J. Bolton, Mater. High Temp. 31 (2014) 109–120.
[10] J. Bolton, Int. J. Pressure Vessels Pip. 157 (2017) 1–19.
[11] D.W. MacLachlan, D.M. Knowles, Mater. Sci. Eng. A 302 (2001) 275–285.
[12] S.C. Prasad, K.R. Rajagopal, I.J. Rao, Acta Mater. 54 (2006) 1487–1500.
[13] R. Oruganti, M. Karadge, S. Swaminathan, Acta Mater. 59 (2011) 2145–2155.
[14] K. Zhang, J.P. Tan, W. Sun, K. Nikbin, S.T. Tu, J. Mater. Sci. Technol. 137 (2022) 14–25.
[15] Q. Luo, Y.L. Guo, B. Liu, Y.J. Feng, J.Y. Zhang, Q. Li, K. Chou, J. Mater. Sci. Technol. 44 (2020) 171–190.
[16] Y.P. Pang, D.K. Sun, Q.F. Gu, K.C. Chou, X.L. Wang, Q. Li, Cryst. Growth Des. 16 (2016) 2404–2415.
[17] Q. Li, Y.F. Lu, Q. Luo, X.H. Yang, Y. Yang, J. Tan, Z.H. Dong, J. Dang, J.B. Li, Y. Chen, J. Magnes. Alloy. 9 (2021) 1922–1941.
[18] Q. Li, X. Lin, Q. Luo, Y.A. Chen, J.F. Wang, B. Jiang, F.S. Pan, Int. J. Miner. Metall. Mater. 29 (2022) 32–48.
[19] Y.P. Pang, Q. Li, Scr. Mater. 130 (2017) 223–228.
[20] Q. Luo, J.D. Li, B. Li, B. Liu, H.Y. Shao, Q. Li, J. Magnes. Alloy. 7 (2019) 58–71.
[21] R. Ramprasad, R. Batra, G. Pilania, A. Mannodi-Kanakkithodi, C. Kim, npj Computat. Mater. 3 (2017) 54.
[22] K.T. Butler, D.W. Davies, H. Cartwright, O. Isayev, A. Walsh, Nature 559 (2018) 547–555.
[23] P.C. Jennings, S. Lysgaard, J.S. Hummelshøj, T. Vegge, T. Bligaard, npj Comput. Mater. 5 (2019) 46.
[24] H.X. Liu, H.L. Yan, N. Jia, S. Tang, D.Y. Cong, B. Yang, Z.B. Li, Y.D. Zhang, C. Esling, X. Zhao, J. Mater. Sci. Technol. 131 (2022) 1–13.
[25] J.J. He, R. Sandström, J. Zhang, H.Y. Qin, J. Mater. Res. Technol. 22 (2023) 923–937.
[26] D. Shin, Y. Yamamoto, M.P. Brady, S. Lee, J.A. Haynes, Acta Mater. 168 (2019) 321–330.
[27] Y.M. Tan, X.W. Wang, Z.T. Kang, F. Ye, Y.F. Chen, D.W. Zhou, X.C. Zhang, J.M. Gong, J. Mater. Res. Technol. 21 (2022) 4745–4760.
[28] O. Mamun, M. Wenzlick, A. Sathanur, J. Hawk, R. Devanathan, npj Mater. Degrad. 5 (2021) 20.
[29] K. Nakamura, T. Ohnuma, Mater. Today Commun. 36 (2023) 106687.
[30] C.C. Wang, X.L. Wei, D. Ren, X. Wang, W. Xu, Mater. Des. 213 (2022) 110326.
[31] Y. Liu, J.M. Wu, Z.C. Wang, X.G. Lu, M. Avdeev, S.Q. Shi, C.Y. Wang, T. Yu, Acta Mater. 195 (2020) 454–467.
[32] D. Jha, K. Choudhary, F. Tavazza, W.K. Liao, A. Choudhary, C. Campbell, A. Agrawal, Nat. Commun. 10 (2019) 5316.
[33] H. Yamada, C. Liu, S. Wu, Y. Koyama, S.H. Ju, J. Shiomi, J. Morikawa, R. Yoshida, ACS Central Sci. 5 (2019) 1717–1730.
[34] V. Gupta, K. Choudhary, F. Tavazza, C. Campbell, W.K. Liao, A. Choudhary, A. Agrawal, Nat. Commun. 12 (2021) 6595.
[35] Z.Y. Liu, M. Jiang, T.F. Luo, Sci. Adv. 6 (2020) eabd1356.
[36] R.W. Evans, R.J. Hull, B. Wilshire, J. Mater, Process. Technol. 56 (1996) 492–501.
[37] Z.Z. Zheng, S.L. Xiao, X.S. Wang, Y.F. Guo, J.H. Yang, L.J. Xu, Y.Y. Chen, Mater. Sci. Eng. A 803 (2021) 140487.
[38] H. Mishra, P. Ghosal, T.K. Nandy, P.K. Sagar, Mater. Sci. Eng. A 399 (2005) 222–231.
[39] Z.Z. Zheng, F.T. Kong, Y.Y. Chen, X.P. Wang, Mater. Charact. 178 (2021) 111249.
[40] W.Y. Li, Z.Y. Chen, J.R. Liu, Q.J. Wang, G.X. Sui, Mater. Sci. Eng. A 688 (2017) 322–329.
[41] L.A.N.S. Briguente, A.A. Couto, N.M. Guimarães, D.A.P. Reis, C. de Moura Neto, M.J.R. Barboza, in: Proceedings of the 7th International Conference on Diffusion in Solids and Liquids, Algarve, 2011 June 26–30.
[42] G. Singh, D.V.V. Satyanarayana, R. Pederson, R. Datta, U. Ramamurty, Mater. Sci. Eng. A 597 (2014) 194–203.
[43] V.M.C.A. Oliveira, A.M. Vazquez, C. Aguiar, A. Robin, M.J.R. Barboza, Mater. Sci. Eng. A 670 (2016) 357–368.
[44] Z.X. Zhang, J.K. Fan, R.F. Li, H.C. Kou, Z.Y. Chen, Q.J. Wang, H.L. Zhang, J. Wang, Q. Gao, J.S. Li, J. Mater. Sci. Technol. 75 (2021) 265–275.
[45] C.M. Omprakash, D.V.V. Satyanarayana, V. Kumar, Mater. Sci. Technol. 27 (2011) 1427–1432.
[46] D.H. Wolpert, W.G. Macready, IEEE Trans. Evol. Comput. 1 (1997) 67–82.
[47] F.R. Larson, J. Miller, Trans. Am. Soc. Mech. Eng. 74 (1952) 765–771.
[48] I. Balasundar, T. Raghu, B.P. Kashyap, Mater. Sci. Eng. A 609 (2014) 241–249.
[49] M. Es-Souni, Mater. Charact. 46 (2001) 365–379.
[50] T.B. Wang, B.I. Li, Z.Q. Wang, Z.R. Nie, Mater. Sci. Eng. A 731 (2018) 12–20.